Supplemental Materials: Subtemperate sliding reduces inter-Heinrich period in a box model

Logan MANN[1], Colin MEYER[1], Alexander ROBEL[2], Elisa MANTELLI[3,4]

[1]*Thayer School of Engineering, Dartmouth College*

[2]*School of Earth and Atmospheric Sciences, Georgia Institute of Technology*

[3]*Department of Earth and Environmental Sciences, Ludwig-Maximillians-Universitẗ München*

[4]*Glaciology Section, Alfred Wegener Institute Helmholtz Centre for Polar and Marine Research, Bremerhaven, Germany*

Correspondence: Logan Mann <logan.e.mann.th@dartmouth.edu>

ABSTRACT.

S1: R13 MODEL DESCRIPTION

Ice Dynamics

We adapt the ice stream model from Robel and others (2013) (hereafter, R13), a simple box model, which simulates the dynamics and temporal variability of ice stream flow with minimal complexity and little computational expense (described fully in the appendix A1). The R13 model has been used or modified to investigate ice stream variability under the influence of stochastic climate forcings (Mantelli and others, 2016), frozen fringe and sediment freeze-on (Meyer and others, 2019, 2023), and synchronization of Heinrich and DO events through ice ocean interactions (Mann and others, 2021).

R13 couples ice stream hydrology to ice stream dynamics, in a spatially lumped system of ODEs. The ice stream domain is lumped into a rectangle of length L in the along-flow x-direction and width W in the cross-flow y-direction (Figure **??**). Ice thickness is represented as a single spatially lumped average, evolving as a result of a balance between accumulation and transport due to ice stream velocity

$$\frac{dh}{dt} = a_c - \frac{u_b h}{L} \tag{1}$$

where h is the ice thickness, a_c is the accumulation rate, and u_b is the basal velocity

R13 uses an approximation developed by Raymond (1996) to calculate the centerline basal sliding velocity resulting from the Coulomb friction law

$$u_{b,\text{surge}} = \frac{A_g W^{n+1}}{4^n (n+1) h^n} \max(\tau_d - \tau_y, 0)^n. \tag{2}$$

where A_g is the Glen's law coefficient, n is the Glen's law exponent, set here as $n = 3$, although recent studies suggest $n = 4$ may be more accurate for fast extensional ice flow (Millstein and others, 2022), W is the width of the ice stream, and h is the thickness. Surges may occur when driving stress, $\tau_d = \rho g \frac{h^2}{L}$ exceeds the till strength, $\tau_y = \mu N$, where N is the effective pressure and μ is a friction coefficient. We express this relationship directly in terms of the void ratio, e, which has a consolidation threshold, e_c

$$\tau_y = a' \exp\left[-b(e - e_c)\right] \tag{3}$$

where a' is the till strength at consolidation and b is an empirical constant. e is a diagnostic variable resulting from the subglacial hydrology model, used in R13.

We introduce subtemperate sliding to R13, by selecting a function $f(T_b)$ for equation (**??**), which aims to parameterize the velocity at freezing temperatures, which increases as the bed temperature approaches the melting point, because the thickness of premelted water films increases with temperature (Wettlaufer and Worster, 2006). We choose an exponential empirical relation, from Mantelli and Schoof (2019b), i.e.

$$u_{b,\text{subtemp}} = C \exp\left[(T_b - T_m)/T_0\right] \tau_b^m \tag{4}$$

where, C is a friction coefficient, m is the sliding exponent, T_b is the temperature at the base, T_m is the melting temperature, and T_0 determines the range below the melting point in which subtemperate sliding is active. The subtemperate sliding velocity here is a function of basal shear stress, τ_b, which balances driving stresses, τ_d when the ice is frozen to the bed.

Assuming that $u_{b,\text{subtemp}} \ll u_{b,\text{surge}}$ during a surge, these flow laws can be combined, such that subtemperate sliding dominates basal sliding velocity when $\tau_d < \tau_y$ and the surge velocity dominates when $\tau_d > \tau_y$.

$$u_b = \left[C + \frac{A_g W^{n+1}}{4^n (n+1) h^n \tau_b^m} \max(\tau_d - \tau_y, 0)^n \right] \exp[(T_b - T_m)/T_0] \tau_b^m. \tag{5}$$

In the stagnant phase, when $\tau_d < \tau_y$, the till is completely frozen ($T_b < T_m$), and the surge component is inactive. During till failure, when $\tau_d > \tau_y$, the bed is temperate ($T_b = T_m$), the till is saturated to a critical level, and the subtemperate sliding term is negligible compared to the surge term. There is a seamless

transition between the Weertman-style sliding law governing subtemperate sliding in equation (4) and the Coulomb friction law governing till failure and surge in equation (2). When the till is frozen, subtemperate sliding is resisted by the basal shear stress, τ_b, which is balanced by the driving stress τ_d, but during till failure, basal shear stress is balanced the till strength τ_y, which is exceeded by the driving stress τ_d

$$\tau_b = \begin{cases} \tau_y & \text{if } \tau_d > \tau_y \\ \tau_d & \text{otherwise} \end{cases} . \tag{6}$$

Thermal and Hydrology Model

The ice stream model from R13, described in the body of the main text is coupled to a subglacial hydrology model, which is also a spatially lumped model. Meltwater content w is related to the void ratio, e and till thickness, Z_s, through $w = eZ_s$, and is calculated prognostically through a balance of meltwater production and drainage. When w is positive,

$$\frac{dw}{dt} = m - \frac{Q_d}{LW}, \tag{7}$$

where m is the basal melt rate, Q_d is the rate of volumetric discharge. m is determined through basal heat flux, G, conduction through the ice to the atmosphere, and frictional heat from sliding.

$$m = \frac{1}{\rho_i L_f}\left[G + \frac{k_i(T_s - T_b)}{h} + \tau_b u_b\right], \tag{8}$$

where ρ_i is the density of ice, L_f is the latent heat of fusion, k_i is the thermal conductivity of ice, T_s is the atmospheric temperature, held constant throughout model runs, T_b is the temperature at the ice base, τ_b is the basal shear stress. A positive m indicates melting, and a negative m indicates freezing. When the till water content reaches saturation, we assume that all additional meltwater is drained,

$$Q_d = \begin{cases} 0 \text{ if } w < w_s \text{ or } m < 0 \\ mLW \text{ otherwise} \end{cases} , \tag{9}$$

This hydrology ultimately determines sliding from till deformation (see eq (2)).

At low void ratios, a frozen fringe propagates through the sediments, until the till thickness, Z_s is reduced to 0 at $e = e_c$,

$$\frac{dZ_s}{dt} = \begin{cases} 0 \text{ if } e > e_c \text{ or } Z_s = 0 \\ \frac{m}{e_c} \text{ if } e = e_c \text{ and } Z_0 > Z_s > 0 \end{cases} , \tag{10}$$

where Z_0 is the maximum sediment thickness. When the till layer is completely frozen, $Z_s = 0$ and basal ice can cool, reducing the vertical temperature gradient. The bed temperature evolves according to the thermal model in R13, which spatially lumps the heat equation

$$\begin{cases} T_b = T_m \text{ if } w > 0 \\ \frac{dT_b}{dt} = \frac{\rho_i L_f}{C_i h_b} m \text{ if } w = 0 \text{ and either } (T_b = T_m \text{ and } m < 0) \text{ or } (T_b < T_m) \end{cases} \tag{11}$$

where C_i is the heat capacity of ice, h_b is the thickness of the temperate basal ice layer, G is the geothermal heat flux, k_i is the thermal conductivity of ice, and T_s is the surface temperature. The frictional heating term, $\tau_b u_b$, bidirectionally couples our ice flow model to the thermal model, allowing for the possibility of thermal feedbacks between sliding and bed temperature. As we will see in this study, the inclusion of subtemperate sliding implies frictional heat between surges. This nonlinear coupling can amplify small perturbations in the ice flow model from R13, causing major changes in ice stream behavior.

S2: STABILITY ANALYSIS

Scaling

Taking the scales from Robel and others (2013),

$$[h] = \frac{a_c L}{[u_b]} = L \left[\frac{A_g W^{n+1} (\rho_i g)^n}{4^n (n+1) a_c} \right]^{\frac{-1}{(n+1)}} \tag{B1}$$

$$[t] = [h]/a_c = \frac{L}{a_c} \left[\frac{A_g W^{n+1} (\rho_i g)^n}{4^n (n+1) a_c} \right]^{\frac{-1}{(n+1)}} \tag{B2}$$

$$\begin{aligned} [u_b] = [u_{b,\text{surge}}] = [u_{b,\text{subtemp}}] &= \frac{a_c L}{[h]} \\ &= \frac{A_g W^{n+1}}{4^n (n+1)} \left(\frac{[\tau_d]}{[h]} \right)^n = a_c \left[\frac{A_g W^{n+1} (\rho_i g)^n}{4^n (n+1) a_c} \right]^{\frac{1}{(n+1)}} \end{aligned} \tag{B3}$$

$$[\tau_d] = [\tau_b] = [\tau_y] = \frac{\rho_i g [h]^2}{L} = \rho_i g L \left[\frac{A_g W^{n+1} (\rho_i g)^n}{4^n (n+1) a_c} \right]^{\frac{-2}{(n+1)}} \tag{B4}$$

$$[m] = \frac{[u_b][\tau_b]}{\rho_i L_f} = \frac{a_c g L}{L_f} \left[\frac{A_g W^{n+1} (\rho_i g)^n}{4^n (n+1) a_c} \right]^{\frac{-1}{(n+1)}} \tag{B5}$$

$$[Q_d] = [m] L W = \frac{a_c g}{W L_f} \left[\frac{A_g W^{n+1} (\rho_i g)^n}{4^n (n+1) a_c} \right]^{\frac{-1}{(n+1)}} \tag{B6}$$

Parameter	Description	Value	Unit
a'	Till empirical coefficient	1.41×10^6	[Pa]
a_c	Accumulation rate	0.1	[m yr^{-1}]
A_g	Glen's law rate factor	5×10^{-25}	[Pa^{-n} s^{-1}]
b	Till empirical exponent	21.7	[Unitless]
C_i	Volumetric heat capacity of ice	1.94×10^6	[J K^{-1} m^{-3}]
e_c	Till consolidation thresshold	0.3	[unitless]
g	Gravitational acceleration	9.81	[m s^{-2}]
G	Geothermal heat flux	0.03	[W m^{-2}]
h_b	Thickness of temperate ice layer	10	[m]
k_i	Thermal conductivity of ice	2.1	[J s^{-1} m^{-1} K^{-1}]
L	Ice stream trunk length	500	[km]
L_f	Specific latent heat of ice	3.35×10^5	[J kg^{-1}]
m	Subtemperate Sliding Law Exponent	1	[unitless]
n	Glen's law exponent	3	[unitless]
T_m	Melting point of ice	0	[°C]
T_s	Surface temperature	-30	[°C]
T_0	Temp. range of subtemperate sliding	10	[°C]
W	Ice stream trunk width	40	[km]
w_s	Till saturation threshold	1	[m]
Z_0	Initial effective till layer thickness	1	[m]
ρ_i	Ice density	917	[kg m^{-3}]
ρ_w	Water density	1000	[kg m^{-3}]

Table 1. Paramters used in the defualt, subtemperate sliding model

$$[T_b] = T_m \tag{B7}$$

$$[w] = w_s \tag{B8}$$

$$[e] = e_c \tag{B9}$$

$$[Z_s] = \frac{[w]}{[e]} = \frac{w_s}{e_c} \tag{B10}$$

Nondimensional Groups:

$$\alpha = \frac{[w]}{[m][t]} = \frac{w_s L_f}{L^2 g}\left[\frac{A_g W^{n+1}(\rho_i g)^n}{4^n(n+1)a_c}\right]^{\frac{2}{(n+1)}} \tag{B11}$$

$$\beta = \frac{G}{[\tau_b][u_b]} = \frac{G}{a_c \rho_i g L}\left[\frac{A_g W^{n+1}(\rho_i g)^n}{4^n(n+1)a_c}\right]^{\frac{1}{(n+1)}} \tag{B12}$$

$$\gamma = \frac{k_i(T_m - T_s)}{[h][\tau_b][u_b]} = \frac{k_i(T_m - T_s)}{a_c \rho_i g L^2}\left[\frac{A_g W^{n+1}(\rho_i g)^n}{4^n(n+1)a_c}\right]^{\frac{2}{(n+1)}} \tag{B13}$$

$$\nu = \frac{T_m C_i h_b}{[t][\tau_b][u_b]} = \frac{T_m C_i h_b}{\rho_i g L^2}\left[\frac{A_g W^{n+1}(\rho_i g)^n}{4^n(n+1)a_c}\right]^{\frac{2}{(n+1)}} \tag{B14}$$

$$\delta = \frac{a'}{[\tau_d]} = \frac{a'}{\rho_i g L}\left[\frac{A_g W^{n+1}(\rho_i g)^n}{4^n(n+1)a_c}\right]^{\frac{2}{(n+1)}} \tag{B15}$$

$$\xi = C^{-1}\frac{[\tau_d]^m}{[u_b]} = \frac{(\rho_i g L)^m}{C a_c}\left[\frac{A_g W^{n+1}(\rho_i g)^n}{4^n(n+1)a_c}\right]^{\frac{-2m-1}{(n+1)}} \tag{B16}$$

Prognostic Equations: Asterisks dropped for convenience

$$\frac{dh}{dt} = 1 - u_b h \tag{B17}$$

$$\alpha\frac{dw}{dt} = \begin{cases} m \text{ if } w < 1 \text{ or } m < 0 \\ 0 \text{ otherwise} \end{cases} \tag{B18}$$

$$\alpha\frac{dZ_s}{dt} = \begin{cases} 0 \text{ if } e > 1 \text{ or } z_s = 0 \\ m \text{ if } e = 1 \text{ and } Z_0 e_c / w_s > Z_s > 0 \end{cases} \tag{B19}$$

$$\begin{cases} T_b = 1 \text{ if } w > 0 \\ \nu \frac{dT_b}{dt} = m \text{ if } w = 0 \text{ and either } (T_b = 1 \text{ and } m < 0) \text{ or } (T_b < 1) \end{cases} \tag{B20}$$

Diagnostic Equations:

$$m = \beta + \gamma \frac{T_s - T_m T_b}{h(T_m - T_s)} + \tau_b u_b \tag{B21}$$

$$\tau_d = (h)^2 \tag{B22}$$

$$\tau_y = \delta \exp\left[-b e_c (e-1)\right] \tag{B23}$$

$$\tau_b = \begin{cases} \tau_y \text{ if } \tau_d > \tau_y \\ \tau_d \text{ otherwise} \end{cases} \tag{B24}$$

$$u_b = \left[\xi(\tau_b)^m + \max(h - \frac{\tau_y}{h}, 0)^n \right] \exp\left[T_m (T_b - 1)/T_0 \right] \tag{B25}$$

Undrained System

In the supplemental materials of Robel and others (2013), model is reduced to the undrained regime (i.e. $w > 0$, $T_b = T_m$, $\dot{Z}_s = 0$), for the purposes of locating the Hopf bifurcation. Note the following changes to the system:

$$\frac{dh}{dt} = 1 - h u_b \tag{B26}$$

$$\alpha \frac{dw}{dt} = \begin{cases} m \text{ if } w < 1 \text{ or } m < 0 \\ 0 \text{ otherwise} \end{cases} \tag{B27}$$

$$m = \beta - \gamma/h + \tau_b u_b \tag{B28}$$

$$\tau_d = (h)^2 \tag{B29}$$

$$\tau_y = \delta \exp\left[-b e_c (e-1)\right] \tag{B30}$$

$$\tau_b = \begin{cases} \tau_y \text{ if } \tau_d > \tau_y \\ \tau_d \text{ otherwise} \end{cases} \tag{B31}$$

$$u_b = \xi \tau_b^m + \max\left[h - \frac{\tau_y}{h}, 0\right]^n \tag{B32}$$

Location of Hopf bifurcation (stability boundary)

It has been of interest to determine whether subtemperate sliding can impact the transition between steady streaming and oscillatory modes. Numerical results indicate that the influence of subtemperate sliding is minimal. In this section we will derive the location of the stability boundary and show that subtemperate sliding is asymptotically small in it's influence on this boundary. Following the analysis in the supplement of Robel and others (2013), the transition between steady streaming and oscillations is a Hopf bifurcation. Assuming the system is not degenerate, we can determine the stability from the trace of the jacobian (which is proportional to the real parts of the eigenvalues).

$$S_t \equiv \mathrm{Tr}(J) = \left.\frac{dF_1}{dh}\right|_{h_0,w_0} + \left.\frac{dF_2}{dw}\right|_{h_0,w_0} \tag{B33}$$

where $F_1 = \frac{dh}{dt}$, $F_2 = \frac{dw}{dt}$. h_0 and w_0 are fixed points. At $S_t = 0$, the system undergoes a subcritical Hopf bifurcation from a stable fixed point ($S_t < 0$) to a stable limit cycle ($S_t > 0$). By setting $S_t = 0$, we can find the transition.

We find the fixed points as

$$0 = 1 - h u_b \tag{B34}$$

$$0 = \tau_b u_b + \beta - \gamma/h \tag{B35}$$

where

$$u_b = \xi \tau_b^m + \left(h - \frac{\tau_b}{h}\right)^n \tag{B36}$$

However, because $\xi \sim O(10^{-2})$, $\tau_b \sim O(1)$, and $h \sim O(1)$ the second term dominates. So, continue the stability analysis of Robel and others (2013), with

$$u_b = (h - \tau_b/h)^n \tag{B37}$$

substitute (B37) into equations (B34-B35) and solve for τ_b

$$\tau_b = h^2 - h^{\frac{n-1}{n}} \tag{B38}$$

$$\tau_b = \gamma - \beta h \tag{B39}$$

Equate for an expression of fixed point, h_0

$$(h_0)^2 + \beta h_0 - (h_0)^{\frac{n-1}{n}} - \nu = 0 \tag{B40}$$

Returning to the stability parameter S_t, we have

$$S_t = \frac{d}{dh}(1 - hu) + \frac{d}{dw}\left(\frac{\tau_b u_b + \beta - \gamma/h}{\alpha}\right) \tag{B41}$$

We determine the scales of each term

$$\frac{d}{dh}(1 - hu) \sim O(1) \tag{B42}$$

$$\frac{d}{dw}\left(\frac{\tau_b u_b + \beta - \gamma/h}{\alpha}\right) \sim O\left(\alpha^{-1}\right) \tag{B43}$$

because $\alpha \sim O(10^{-1})$, the second term dominates. We differentiate

$$S_t = \frac{d}{dw}\left(\frac{\tau_b u_b + \beta - \gamma/h}{\alpha}\right) \tag{B44}$$

$$= \frac{1}{\alpha}\left[- \delta b \tau_b u_b + \frac{n\delta b \tau_b^2}{h}(h - \tau_b/h)^{n-1}\right] \tag{B45}$$

$$= \frac{\delta b \tau_b u_b}{\alpha}\left[\frac{n\tau_b}{h^2 - \tau_b} - 1\right] \tag{B46}$$

We set $S_t = 0$ to determine the location of the Hopf bifurcation

$$0 = \frac{\delta b \tau_b u_b}{\alpha}\left[\frac{n\tau_b}{h^2 - \tau_b} - 1\right] \tag{B47}$$

$$h^2 - (n+1)\tau_b = 0 \tag{B48}$$

We substitute (B39)

$$h^2 - (n+1)(\gamma - \beta h) = 0 \tag{B49}$$

$$h^2 - \gamma(n+1) + \beta(n+1)h = 0 \tag{B50}$$

$$\beta = \frac{\gamma}{h} - \frac{h}{n+1} \tag{B51}$$

With this expression of β, we return to equation (B40) and solve for h

$$h_0^2 + \left(\frac{\gamma}{h_0} - \frac{h_0}{n+1}\right)h_0 - h_0^{\frac{n-1}{n}} - \gamma = 0 \tag{B52}$$

$$h_0^2 - \frac{h_0^2}{n+1} - h_0^{\frac{n-1}{n}} = 0 \tag{B53}$$

$$h_0 = \left(\frac{n+1}{n}\right)^{-\frac{n}{n+1}} \tag{B54}$$

Thus, the stability boundary is,

$$\beta = \left(\frac{n+1}{n}\right)^{-\frac{n}{n+1}} \gamma - \frac{\left(\frac{n+1}{n}\right)^{\frac{n}{n+1}}}{n+1} \tag{B55}$$

controlled only by the nondimensional groups β (geothermal heat) and α (conduction through to surface), as shown in Robel and others (2013). Here we have shown that the influence of subtemperate sliding is minimal to the stability boundary, precisely because the stability boundary occurs in regions of parameter space where subtemperate sliding is asymptotically insignificant in its influence on the system, i.e. oscillations over a temperate bed. [***note: I could probably do the stability analysis, without ignoring subtemperate sliding, but it reduces to a challenging nonlinear algebra problem that may require numerical root finding. Instead, I've just made an argument for dropping it up front, but this isn't necessarily anything new. Another thought, there is another internal dynamical boundary inside the oscillatory mode, between 'temperate oscillations', where the bed is at the melting point for most of the stagnant period, thus being governed only by the undrained model, and 'subtemperate oscillations' where the bed is frozen for most of the stagnant period causing a much greater dependency on subtemperate sliding. Could we find this boundary analytically and compare to our results?]

S3: SUBTEMPERATE SLIDING PARAMETERIZATIONS

In the main text, the premelting temperature range is set to $T_0 = 1$ °C below the melting point. While some studies have observed subtemperate sliding for basal temperatures as low as -17 °C (Cuffey and others, 1999), the analysis of Mantelli and Schoof (2019b), as well as Schoof and Mantelli (2021), suggest that subtemperate sliding should occur within a very small range compared to the scale of temperature variability. Either way, T_0 is a very significant unconstrained parameter. Further, the exponential functional description of subtemperate sliding, $g(T_b) = \exp(T_b - T_m)/T_0$, proposed in Mantelli and Schoof (2019b) is not an empirical relationship, constrained by observations. Rather, it is introduced as a possible option to regularize the subtemperate sliding which Mantelli and others (2019a) prove must occur.

We hypothesize that any parameterization which captures the basic relationship between increased basal temperature and increased sliding velocity should have a capacity for thermal feedback at the bed. Yet, the

dependence of our results on this parameterization must be explored. To this end, we perform 4 experiments, catalogued in Figure (1), aimed at determining: 1) The effect of the premelting temperature range, T_0, on our results, and 2) The effect of our functional parameterization of subtemperate sliding. Next we perform parameter sweeps for a range of values of T_0 from 0.1 to 10 °C on a logarithmic scale (Figures 3-4). These experiments show that: 1) subtemperate sliding can generate robust thermal and hydraulic feedbacks, even within a small range of the melting temperature, and 2) that this mechanism exhibits some degree of path-independence with respect to the specific functional parameterization chosen, meaning that the temperature at which subtemperate sliding occurs in significant amounts largely determines the event period, rather that the specific function chosen. However, future theoretical, experimental, and observational work should be conducted to constrain premelt and subtemperate sliding parameterizations for ice sheet models. The results of our study indicate that this parameterization may be fundamentally important for projecting ice loss and sea level rise from the Antarctic Ice sheet.

Effect of T_0

In experiments A and B, we examine the effects of subtemperate sliding for different values of T_0, but with the same subtemperate sliding parameter $\xi = 0.01$. Experiment A is meant to represent a premelting temperature range that is asymptotically very small compared to the range of temperature variation $O(10^{-3})$, as suggested by theoretical results. By contrast, experiment B is meant to represent subtemperate sliding at very low basal temperatures, which some observations suggest may be possible Cuffey and others (1999).

In Experiment A (Figure 2a-c), the onset of subtemperate sliding occurs around -0.1 °C, and rapidly increases in speed. Without the inclusion of the subglacial hydrology model, this result would be similar to the no-slip scenario. However, once the bed reaches the melting point, subtemperate sliding is still active at its maximum value, determined by $\xi = 0.01$. The subsequent heat dissipation during the short period during which the bed is temperate, but the till has not yet failed, accelerates meltwater generation and the onset of till failure. Thus, this scenario still leads to a $\sim 22\%$ reduction in event period, with most of this reduction occurring during the period between a temperate bed and the onset of till failure.

In experiment B (Figure 2d-e), the onset of subtemperate sliding occurs around 10 °C, and rapidly increases in speed. Thus this scenario alters the thermal trajectory considerably and reduces the time between the onset of a temperate bed and the onset of till failure, leading to a $\sim 46\%$ reduction in event period.

In figure 3, we repeat the parameter sweep from main text figure 3, for a range of values of T_0 from 0.1 to 10 °C on a logarithmic scale (Figures 3-4). We see that subtemperate sliding substantially decreases event period across parameter space, even for very small T_0, but the weak oscillatory region is unaffected by this change. This is because weak oscillations are characterized by hydraulic feedbacks, caused by sliding during the stagnant phase over a temperate bed. Thus, the premelting temperature range has no impact on this phase. In stead, the friction parameter xi controls the change in the temperate, but not yet surging, phase. This effect means that for smaller ranges of T_0, the bifurcation between strong and weak oscillations is particularly stark.

These experiments and parameter sweeps lead to an intuitive conclusion, that higher premelting temperature ranges lead to higher decreases in event period, particularly in the strong oscillatory regimes. However, even very small premelting temperature ranges lead to significant decreases in event period. This is because of both thermal feedbacks in the subtemperate phase and hydrological feedbacks in the temperate, yet still stagnant, phase. The relative importance of the subtemperate phase vs. the temperate stagnant phase varies depending on parameterization.

Effect of subtemperate sliding parameterization

Next, we are interested in the sensitivity of the model to alternative parameterizations of subtemperate sliding. For comparison, we consider a scenario where the acceleration of subtemperate sliding rapidly increases as it approaches a critical temperature, T_c, below the melting point, then the acceleration of sliding decreases at the bed temperature increases. The range of acceleration/deceleration is determined by T_0. We give a functional description to this behavior as

$$g(T_b) = \frac{1}{2} + \frac{1}{2}\tanh\frac{T_b - T_m - T_c}{T_0} \tag{B56}$$

Here we are interested in determining if the results of our study are highly sensitive to the functional parameterization itself. I.e., is the exponential parameterization introduced by Mantelli and Schoof (2019b) adequate? If a decrease in the rate of acceleration after a critical temperature drastically changes our results from the main text, that the functional parameterization itself takes on a new importance. By contrast, if it does not, then future work should be concerned more with deriving correct parameters for the exponential parameterization, as it will likely capture all of the neccessary features of temperature dependent subtemperate sliding for larger-scale ice sheet modeling.

In experiment C (Figure 5a-b), the critical temperature, T_c, is set to -1 °C and the acceleration-decceleration range, T_0, is set to 1 °C. This scenario is most directly similar to the main text. This leads to a slightly smaller reduction in subtemperate sliding from the main text.

In experiment D, the critical temperature, T_c, is set to -10 °C, and the acceleration-decceleration range, T_0, is set to 10 °C. This scenario is more analogous to experiment B. This also leads to a smaller reduction in subtemperate sliding than experiment B.

With the tanh parameterization, $g(T_b)$ never reaches 1. So in a sense, this parameterization effectively reduces the amount of subtemperate sliding in the temperate bed, pre-surge, phase. This likely accounts for the slightly longer event periods. Examining the thermal trajectories of these experiments reveal a picture that is largely indistinguishable from the exponential experiments.

Therefore, while the specific functional form of subtemperate sliding parameterization does have some effect on the system, results should be similar as long as the model captures the essential relationship between increased basal temperature and increased sliding velocity, that the maximum subtemperate sliding speed is set by a frictional parameter, ξ, and the onset of significant subtemperate sliding occurs at a certain temperature below the melting point, either T_0 or T_c depending on the parameterization. While future work should proceed cautiously, especially given that the exponential parameterization is not empirically derived, it is probably adequate for basic research.

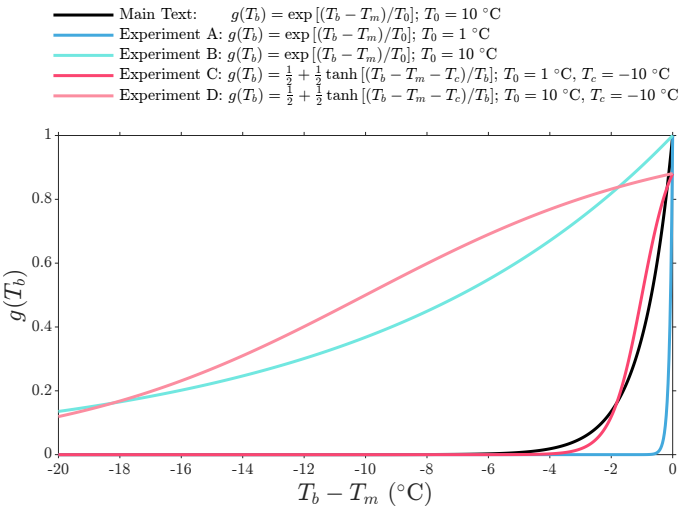

Fig. 1. compares the subtemperate sliding parameterizations, $g(T_b)$, considered in the main text and in the supplementary materials.

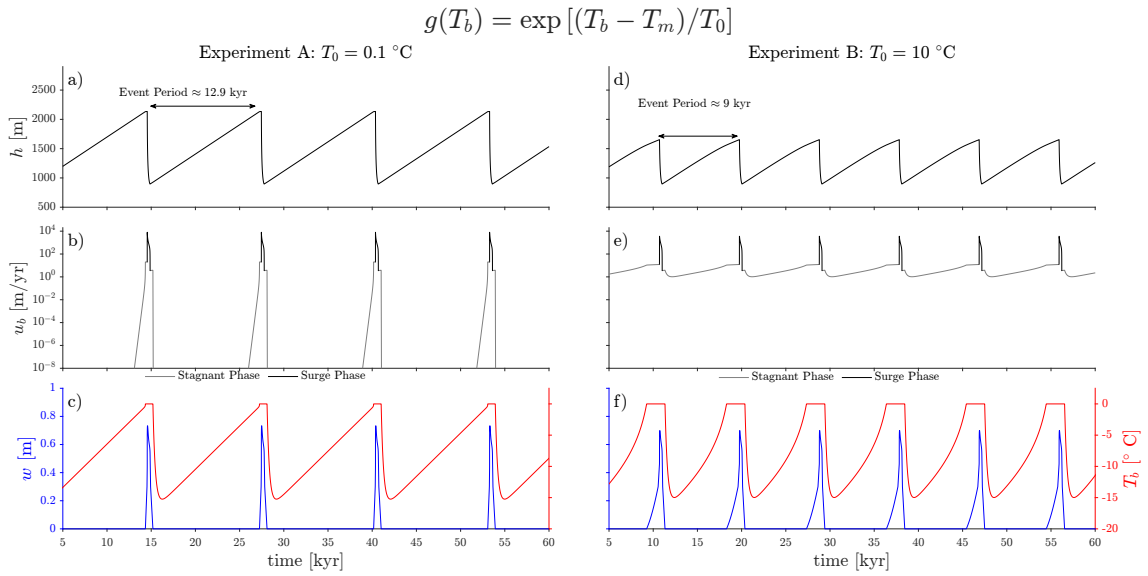

Fig. 2. [Left Column] (a-c) depicts the case of no subtemperate sliding ($\xi = 0$). [Right Column] (d-f) depicts the case of modest subtemperate sliding ($\xi = 0.01$). [First Row] Ice thickness, h. [Second Row] Subglacial slip velocity, u_b, plotted on a logarithmic scale. [Third Row] subglacial water content (blue), w, and Bed Temperature (red), T_b. Parameters: Surface Temperature, $T_s = -30$ °C, Geothermal heat, $G = 0.03$ W/m^2, Premelting temperature range, $T_s = 1$ °C. All variables plotted as a function of time.

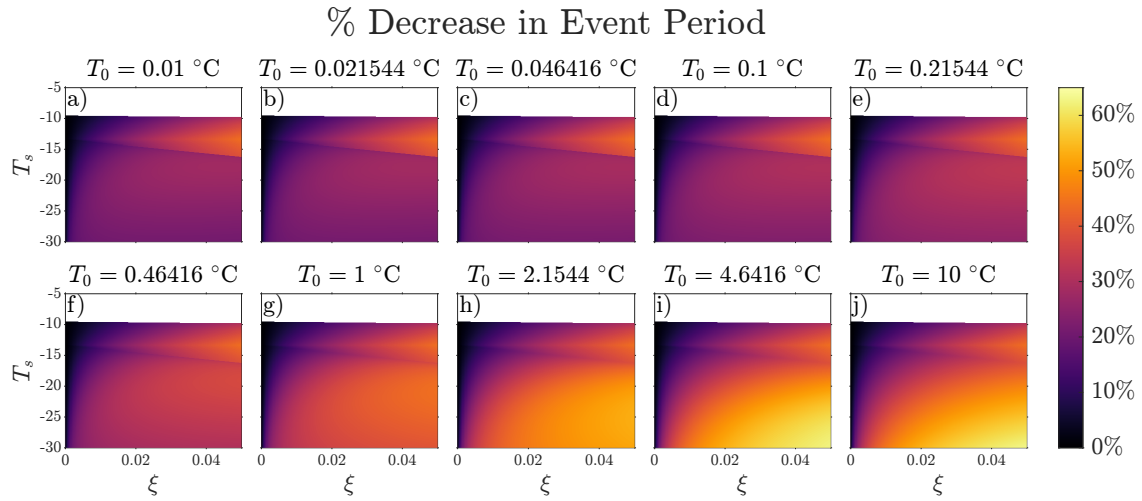

Fig. 3. a-j) Repeating the parameter sweep from the main text with different premelting temperature ranges, ascending in a logarithmic scale from 0.1 to 10.

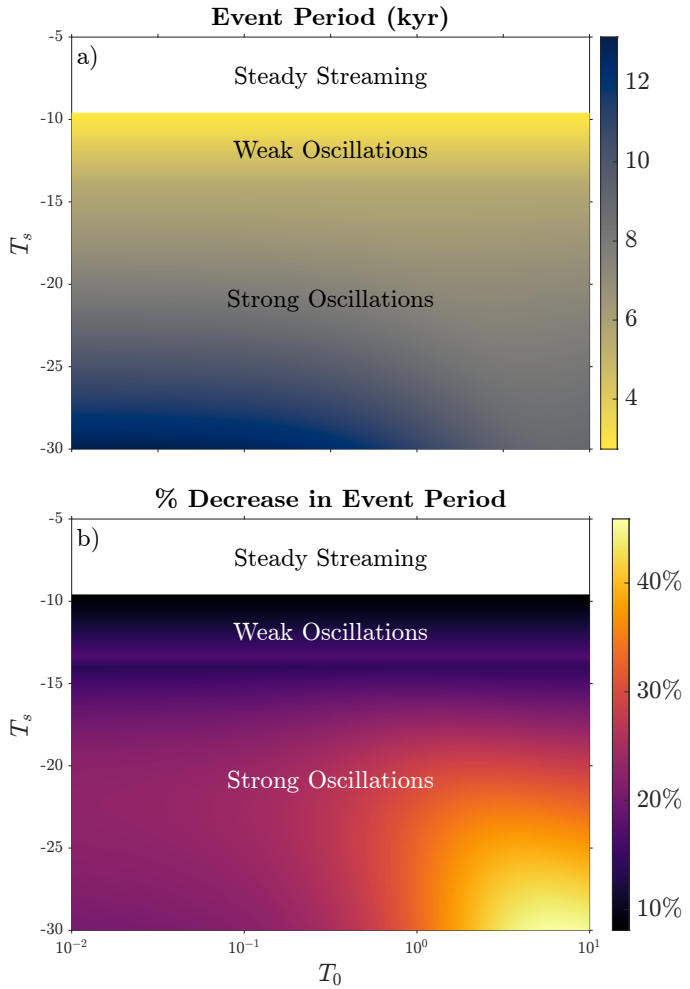

Fig. 4. Parameter sweep for T_0 vs. T_s. a) Event period. b) % decrease in event period

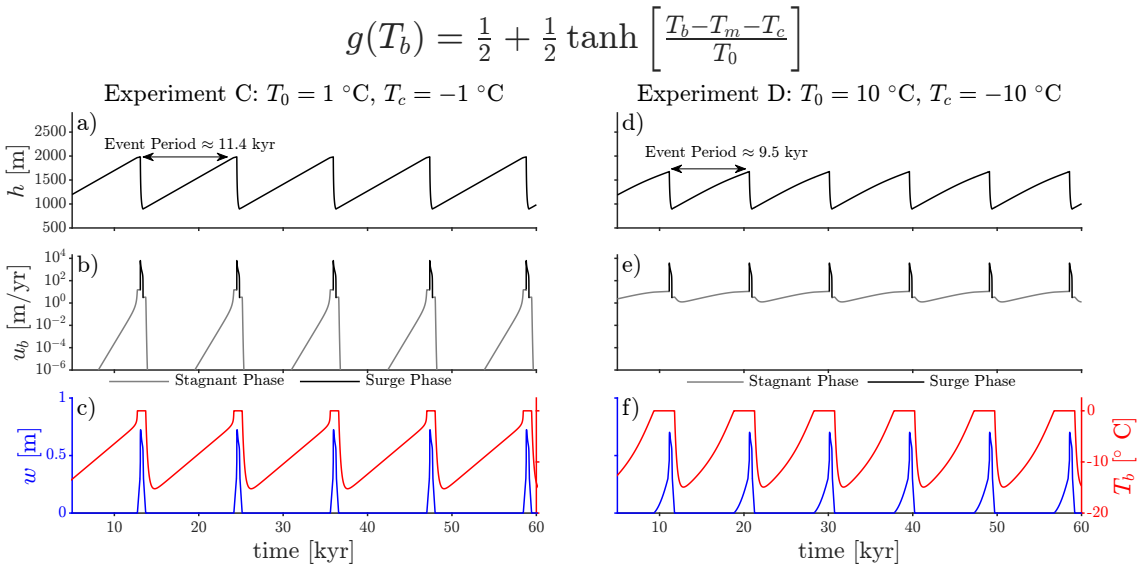

Fig. 5. [Left Column] (a-c) Experiment C ($T_0 = 1$ °C, $T_c = -1$ °C). [Right Column] (d-f) Experiment D ($T_0 = 10$ °C, $T_c = -10$ °C). [First Row] Ice thickness, h. [Second Row] Subglacial slip velocity, u_b, plotted on a logarithmic scale. Note that a cutoff is imposed at 10^{-8} [m/yr], for the purpose of plotting 0 velocity in the no-slip case. [Third Row] subglacial water content (blue), w, and Bed Temperature (red), T_b. Parameters: Surface Temperature, $T_s = -30$ °C, Geothermal heat, $G = 0.03$ W/m^2, Premelting temperature range, $T_s = 1$ °C. All variables plotted as a function of time.

REFERENCES

Cuffey K, Conway H, Hallet B, Gades A and Raymond C (1999) Interfacial water in polar glaciers and glacier sliding at- 17° c. *Geophysical Research Letters*, **26**(6), 751–754

Mann LE, Robel AA and Meyer CR (2021) Synchronization of heinrich and dansgaard-oeschger events through ice-ocean interactions. *Paleoceanography and Paleoclimatology*, **36**(11), e2021PA004334

Mantelli E and Schoof C (2019b) Ice sheet flow with thermally activated sliding. part 2: the stability of subtemperate regions. *Proceedings of the Royal Society A*, **475**(2231), 20190411

Mantelli E, Bertagni MB and Ridolfi L (2016) Stochastic ice stream dynamics. *Proceedings of the National Academy of Sciences*, **113**(32), E4594–E4600

Mantelli E, Haseloff M and Schoof C (2019a) Ice sheet flow with thermally activated sliding. part 1: the role of advection. *Proceedings of the Royal Society A*, **475**(2230), 20190410

Meyer CR, Robel AA and Rempel AW (2019) Frozen fringe explains sediment freeze-on during heinrich events. *Earth and Planetary Science Letters*, **524**, 115725

Meyer CR, Schoof C and Rempel AW (2023) A thermomechanical model for frost heave and subglacial frozen fringe. *Journal of Fluid Mechanics*, **964**, A42

Millstein JD, Minchew BM and Pegler SS (2022) Ice viscosity is more sensitive to stress than commonly assumed. *Communications Earth & Environment*, **3**(1), 57

Raymond C (1996) Shear margins in glaciers and ice sheets. *Journal of Glaciology*, **42**(140), 90–102

Robel AA, Degiuli E, Schoof C and Tziperman E (2013) Dynamics of ice stream temporal variability: Modes, scales, and hysteresis. *Journal of Geophysical Research: Earth Surface*, **118**(2), 925–936

Schoof C and Mantelli E (2021) The role of sliding in ice stream formation. *Proceedings of the Royal Society A*, **477**(2248), 20200870

Wettlaufer JS and Worster MG (2006) Premelting dynamics. *Annu. Rev. Fluid Mech.*, **38**, 427–452